

Chapter X. Electrodes of Cylindrical Geometrical Aspect

10.1 Introduction and Motivation

Electrokinetic remediation cells can be divided in two main zones of interest for its study; this is the treatment zone and the zone near the electrode. The treatment zone, where the highest concentration of contaminant species is usually found, is object of analysis to evaluate the efficiency of removal. The electrode zone, sometimes overlooked, is crucial for the success of the process. In fact, this region is the location of the ultimate chemical reaction and the point of fluid extraction for most versions of the electroremediation technology. In particular, the electrode design plays an important role in the process as the shape characteristic has an effect on the hydrodynamics taking place near the electrode. It is not a mere coincidence that typical applications such as Lasagna and Cation Selective Membrane are mostly conceived with electrodes of rectangular or plate geometrical aspects. Other cases, i.e. Ceramic Casting and Electrochemical ion exchange, are mostly associated with tubular or cylindrical geometrical aspects. In fact, the type of technology being applied is coupled to the electrode shape in an appropriate process design. For this reason there is great interest in the study of these particular systems. As rectangular electrode systems were successfully analyzed in the previous chapter, the next logical step is therefore to concentrate on cylindrical systems.

Cylindrical systems offer interesting features that could be analyzed. The effects of radius aspect and Joule heating on the fluid region near the electrode have not been considered in the literature. Furthermore, the effects of applying higher values of differential potentials are also unknown. Several publications have revealed that during field tests temperature developments have occurred (Chilingar et al., 1997; Lageman, 1993; Ho et al.,

1997; Virkutyle et al., 2002; Yeung et al., 1997). Although, this finding clearly suggests a heat transfer problem, the phenomenon is not necessarily well understood.

As a consequence of the above paragraph, this chapter focuses on the role of the Joule heating effect in the zone near electrodes. In addition, this work also analyzes the effects of the electrode radius aspects on the main parameter fields of the system. In other words, this work promotes a basic understanding of the effects of heat generation and electrode shape on removal efficiency of electrokinetic remediation applications. Specific cases of boundary layer flows, with low Reynolds number, in vertical electrodes of cylindrical aspect are analyzed. The analysis has been kept as simple as possible in order to achieve the main objective of this study; however, the key aspects of the heat generation in the electrokinetic remediation processes have been captured.

10.2 Modeling Approach

The methodology proposed by Turnbull (1969) has been successfully applied to a rectangular system of similar characteristics of electrokinetic cells. The boundary layer approach followed by Turnbull included the effects of an electric field across the flow. The same analysis is conducted herein to describe the behavior of a cylindrical electrode system. The approach is an extension, by analogy, of the Turnbull method to a cylindrical system. Furthermore, this approach introduces important modifications to the study conducted by Turnbull. These modifications consider heat generation (source term) and the change of boundary layer to more reliable fluid conditions. Three transport equations are required for the proper representation of the system. These equations are the Navier-Stokes, the heat transfer, and the continuity equations. The resulting model, from the coupling of the previous equations, is simplified by applying the Von Karman boundary layer approximation to obtain the final solution (Whitaker, 1983). The approximation considers the use of approximate expressions for the hydrodynamic velocity and for the temperature profiles as functions of the coordinate variables (Squire, 1938 and Turnbull, 1969).

10.3 System Description

A vertical electrode of cylindrical geometrical aspect is being analyzed. The symmetrical characteristic of the system, as well as the coordinate system utilized in its modeling, allows considering only the radial, r -direction, and axial, x -direction, coordinate components. In other words, the angular coordinate can be neglected to convert this 3D to a 2D system. The electrode surface in contact with the fluid presents a constant temperature T_0 while the fluid outside the boundary layer region has uniform temperature T_∞ . The temperature difference between the wall surface of the electrode and the fluid causes buoyancy driven flows to take place as a thin boundary layer moving tangential to the vertical cylindrical electrode. In particular, the buoyancy phenomenon, also known as free convection, is promoted by density variations proportional to the aforementioned temperature difference.

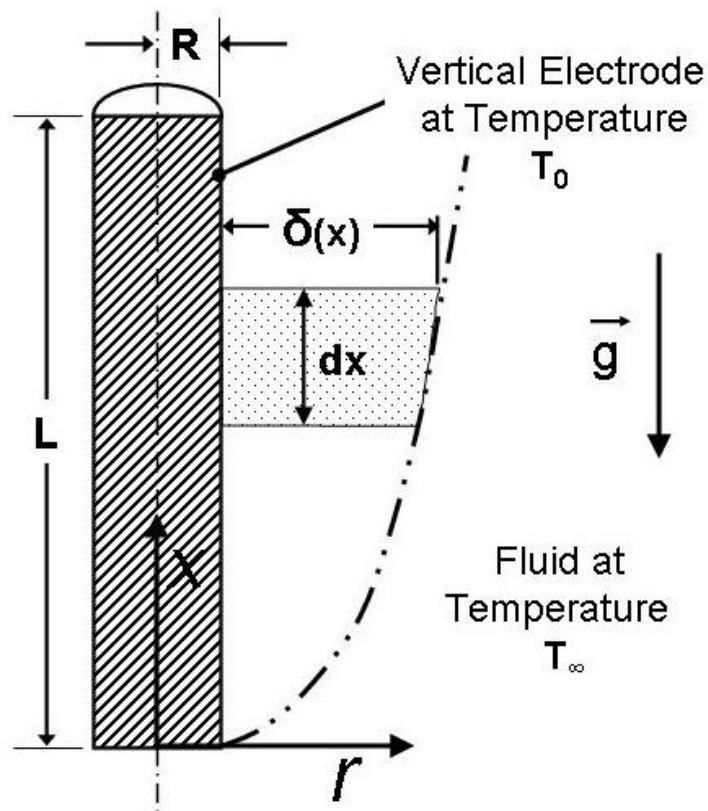


Figure 10.1 Control volume and main variables associated with the boundary layer flow in a cylindrical electrode geometry.

In the radial direction, the r-axis of the chosen coordinates system, an applied electrical field, E, is present stressing the fluid thermodynamic. A Joule heating effect is assumed, inside the boundary layer, as the fluid presents electrical resistance to the electrical field. The heat generated by this thermal stress is of Q in magnitude and assumed constant and uniform with time across the boundary layer. It is also considered that the Joule heating generation could modify further more the hydrodynamic inside the boundary layer of fluid near the cylindrical wall of the electrode. The fluid is assumed Newtonian, incompressible for the mass conservation aspects and under steady state conditions. Furthermore, the Boussinesq (Gebhart et al., 1988) assumption is considered valid in this analysis; this is the fluid has constant physical properties everywhere except for the density in the buoyancy force term.

10.4 Model Formulation

As in the previous chapter, three fundamental equations are needed to theoretical and mathematically described the system under study in terms of temperature and velocity profiles inside the boundary layer. The fundamental expressions that model the system, as presented, are the energy and motion equations. In the present section, these two equations are developed as the heat transfer and hydrodynamic models. However, the use of the continuity equation is crucial to construct the differential mathematical models herein intended.

10.4.1 Heat Transfer Model

Analogously to the approach followed for describing the heat transfer problem in rectangular electrodes, the cylindrical system under study invokes the energy conservation equation (Bird et al., 1960). Since the fluid is considered present electric resistance, a heat generation term must be included in the conservation of energy equation to yield the following general equation:

$$\rho \cdot C_p \frac{DT}{Dt} = \nabla \cdot (k \cdot \nabla T) + Q \quad (10.1)$$

where D is used to indicate the convective derivative, Q is the heat generation due to the Joule heating effect, ρ the fluid density, C_p the specific heat, and k the thermal conductivity of the fluid.

To maintain the analysis as generalized as possible, dimensionless variables are used to conduct the study. Therefore, to transform from X, r coordinate system to a non-dimensional ξ, η system, the following single parameter expressions are introduced:

Thermal Diffusivity

$$\alpha_D = \frac{k}{\rho \cdot C_p} \quad (10.2)$$

Thermal Velocity

$$v_T = \alpha_D \frac{1}{L} \quad (10.3)$$

where L is the electrode length. In particular, introducing the electrode length instead of a characteristic length, as in the case of rectangular electrodes, allows the study of the electrode aspect ratio, a concept that will be introduced later in this chapter.

The following additional definitions of dimensionless variables are also necessary to fully convert the energy equation to dimensionless variables.

$$v_x^+ = \frac{v_x}{v_T} \quad (10.4a)$$

$$v_r^+ = \frac{v_r}{v_T} \quad (10.4b)$$

$$\theta = \frac{T - T_\infty}{T_0 - T_\infty} \quad (10.4c)$$

$$\phi^2 \equiv \frac{Q \cdot L^2}{k \cdot (T_0 - T_\infty)} \quad (10.4d)$$

$$\xi = \frac{x}{L} \quad (10.4e)$$

$$\eta = \frac{r}{L} \quad (10.4f)$$

The trivial substitution of the parameters and variables, previously identified, on equation 10.1 yields the following non-dimensional differential equation for the energy balance.

$$v_x^+ \cdot \frac{\partial \theta}{\partial \xi} + v_r^+ \cdot \frac{\partial \theta}{\partial \eta} = \frac{1}{\eta} \cdot \frac{\partial}{\partial \eta} \left(\eta \cdot \frac{\partial \theta}{\partial \eta} \right) + \phi^2 \quad (10.5)$$

Equation 10.5 is valid for steady state conditions, boundary layer approximation and for heat conduction only important in the radial direction of the system shown in Figure 10.1.

10.4.2 The Continuity Equation

The process, developing near the electrode zone, considers the irreversible conversion of thermal energy in momentum. This phenomenon is observed in the change of the velocity field. The bi-dimensional characteristics the system suggests that the change of velocity in a given direction is achieved at the expense of the other velocity component. This principle comes in the form of the continuity equation for incompressible flow situations; this is $\nabla \cdot \mathbf{v} = 0$ (Bird et al., 1960, Whitaker, 1983). Therefore, for the case of incompressible flow, under the Boussinesq assumption, the following is the expression in cylindrical coordinates.

$$\frac{\partial V_x}{\partial x} + \frac{1}{r} \cdot \frac{\partial}{\partial r} \left(r \cdot \frac{\partial V_r}{\partial r} \right) = 0 \quad (10.6a)$$

or in the dimensionless terms,

$$\frac{\partial V_x^+}{\partial \xi} + \frac{1}{\eta} \cdot \frac{\partial}{\partial \eta} \left(\eta \cdot \frac{\partial V_r^+}{\partial \eta} \right) = 0 \quad (10.6b)$$

10.4.3 Hydrodynamic Model

For this study, it has been assumed that the fluid presents a Newtonian behavior. This assumption leads to representing the hydrodynamic part of the system, as described by the Navier-Stokes equation (Whitaker, 1983). To simplify the analysis in this first effort, none of the electro-mechanisms that normally affect the hydrodynamic field are considered. Therefore, the general expression describing the system is given by

$$\rho \frac{D\mathbf{v}}{Dt} = -\nabla p + \mu \cdot \nabla^2 \mathbf{v} + \rho \cdot \mathbf{g} \quad (10.7)$$

where \mathbf{g} is the gravitational constant, p is the pressure, μ is the fluid viscosity and ρ is the density. Since density is a function of temperature and directly related to convective forces, an explicit expression is required to couple ρ in equation 10.7 with the heat transfer model. The usual approach is to compute the density term as a first order Taylor approximation around a reference temperature T_∞ of the system (Bird et al., 1960, Turnbull, 1969). The explicit expression is given by

$$\rho(T) = \rho(T_\infty) [1 - \beta_\infty \cdot (T - T_\infty)] \quad (10.8)$$

and where β_∞ is the volumetric compressibility of the fluid at a reference temperature T_∞ , in this case the fluid temperature away for the surface of the electrode.

The Navier-Stokes equation (Bird et al, 1960), equation 10.7, can be written in the respective cylindrical components in the x (ξ) and r (η) directions of the system.

Coordinate x :

$$\rho_\infty \cdot \left(v_x \cdot \frac{\partial v_x}{\partial x} + v_r \cdot \frac{\partial v_x}{\partial r} \right) = -\frac{\partial p}{\partial x} - \mathbf{g} \cdot \rho + \mu \cdot \left(\frac{\partial^2 v_x}{\partial \xi^2} + \frac{1}{r} \cdot \frac{\partial}{\partial r} \left(r \cdot \frac{\partial v_x}{\partial r} \right) \right) \quad (10.9a)$$

$$v_x^+ \cdot \frac{\partial v_x^+}{\partial \xi} + v_r^+ \cdot \frac{\partial v_x^+}{\partial \eta} = \frac{1}{\text{Re}} \left(\frac{\partial^2 v_x^+}{\partial \xi^2} + \frac{1}{\eta} \cdot \frac{\partial}{\partial \eta} \left(\eta \cdot \frac{\partial v_x^+}{\partial \eta} \right) \right) + \frac{\text{Gr}}{\text{Re}^2} \theta \quad (10.9b)$$

Coordinate y:

$$\rho_\infty \cdot \left(v_x \cdot \frac{\partial v_r}{\partial x} + v_r \cdot \frac{\partial v_r}{\partial r} \right) = +\mu \cdot \left(\frac{\partial^2 v_r}{\partial x^2} + \frac{1}{r} \cdot \frac{\partial}{\partial r} \left(r \cdot \frac{\partial v_r}{\partial r} \right) \right) \quad (10.10a)$$

$$v_x^+ \cdot \frac{\partial v_r^+}{\partial \xi} + v_r^+ \cdot \frac{\partial v_r^+}{\partial \eta} = \frac{1}{\text{Re}} \left(\frac{\partial^2 v_r^+}{\partial \xi^2} + \frac{1}{\eta} \cdot \frac{\partial}{\partial \eta} \left(\eta \cdot \frac{\partial v_r^+}{\partial \eta} \right) \right) \quad (10.10b)$$

where the following definition of dimensionless numbers applies

$$\text{Gr} = \frac{\rho_\infty^2 \cdot g \cdot \beta_\infty \cdot (T_0 - T_\infty) \cdot L^3}{\mu^2} \quad (10.11a)$$

$$\text{Re} = \frac{\rho_\infty \cdot v_r \cdot L}{\mu} \quad (10.11b)$$

The Grashoff number, Gr, represent the buoyancy to viscous forces due to changes in temperature and density respectively. This free convective phenomenon is shown in equation 10.9 a&b. On the other hand, the Reynolds number, Re, represents the inertia to viscous forces. The Reynolds effect can be observed in both coordinate components, equation 10.9 (a&b) and 10.10 (a&b).

Turnbull's methodology (1969) for rectangular systems has been omitted in the following steps because it does not produce either change or simplification on equations 10.9b and 10.10b. However, Whitaker's idea (1983) can be directly applied obtaining better results. In other words, the simplification proposed by Whitaker is that the order of magnitude of the second derivative with respect to the radial coordinate can be assumed much larger than the one of the second derivative with respect to axial (Whitaker, 1983); this is:

$$\frac{\partial^2(\bullet)}{\partial \eta^2} \gg \frac{\partial^2(\bullet)}{\partial \xi^2} \quad (10.12)$$

This assumption is justified since the width of the boundary layer, δ , is much smaller than any characteristic dimension in the x-direction. In addition, the magnitude of the velocity component, V_x , is considered to be much larger than the one of the other velocity component, V_r .

After applying the simplification suggested by equation 10.12 on equations 10.9b and 10.10b the following expression can be obtained.

Coordinate x:

$$v_x^+ \cdot \frac{\partial v_x^+}{\partial \xi} + v_r^+ \cdot \frac{\partial v_x^+}{\partial \eta} = \frac{1}{\text{Re}} \cdot \frac{1}{\eta} \cdot \frac{\partial}{\partial \eta} \left(\eta \cdot \frac{\partial v_x^+}{\partial \eta} \right) + \frac{\text{Gr}}{\text{Re}^2} \theta \quad (10.13)$$

Coordinate y:

$$v_x^+ \cdot \frac{\partial v_r^+}{\partial \xi} + v_r^+ \cdot \frac{\partial v_r^+}{\partial \eta} = \frac{1}{\text{Re}} \cdot \frac{1}{\eta} \cdot \frac{\partial}{\partial \eta} \left(\eta \cdot \frac{\partial v_r^+}{\partial \eta} \right) \quad (10.14)$$

where all the terms have been previously identified.

Equations 10.13 and 10.14 describe the velocity field of the system under study; however, the driving phenomenon mainly occurs in the axial direction represented by equation 10.13. For that reason, equation 10.13 will be used to describe the convective and buoyancy forces as presented in the next section.

10.5 Derivation of Von Karman Integral Approximation

The target equations to be solved are equations 10.5, for energy, and 10.13, for momentum. As presented, these equations have no trivial solution. The approach, suggested to further simplify this system, is to apply the Von Karman integral approximation in the analysis of the boundary layer. The application of the Von Karman method on equations 10.5 and 10.13 reverses the partial differential equation system, first, to an integro-differential model and, then into a two-equation ordinary differential model (Whitaker, 1983).

According to Von Karman method the target equations need to be integrated over the radial variable (r or η , see Figure 10.1) from the electrode wall surface (i.e., $y = R$, or $\eta=b$) to the edge of the boundary layer, (i.e., $r = R+\delta$, or $\eta = b + \delta^+$). The conditions for the velocity and temperature fields involved in these integrals are

$$V_x^+ = V_r^+ = 0 \quad @ \quad \eta = b \quad (10.15a)$$

$$@ \quad \eta = b + \delta^+ \quad (10.15b)$$

$$\theta = 1 \quad @ \quad \eta = b \quad (10.15c)$$

$$\theta = 0 \quad @ \quad \eta = b + \delta^+ \quad (10.15e)$$

In the suggested mathematical operation, it must be considered that ϕ^2 is constant in the transversal direction, across the boundary layer thickness. As a result, the following integro-differential equations are derived:

$$\frac{\partial}{\partial \xi} \int_b^{b+\delta^+} v_x^+ \cdot \theta \cdot \partial \eta = \int_b^{b+\delta^+} \left(\frac{1}{\eta} \cdot \frac{\partial}{\partial \eta} \cdot \left(\eta \cdot \frac{\partial \theta}{\partial \eta} \right) \right) \cdot \partial \eta + \phi^2 \cdot \delta^+ \quad (10.16)$$

$$\frac{\partial}{\partial \xi} \int_b^{b+\delta^+} (v_x^+)^2 \cdot \partial \eta = \frac{1}{\text{Re}} \cdot \int_b^{b+\delta^+} \left(\frac{1}{\eta} \cdot \frac{\partial}{\partial \eta} \cdot \left(\eta \cdot \frac{\partial v_x^+}{\partial \eta} \right) \right) \cdot \partial \eta + \frac{\text{Gr}}{\text{Re}^2} \cdot \int_b^{b+\delta^+} \theta \cdot \partial \eta \quad (10.17)$$

These are the integral approximations for the energy and momentum equations with a uniform heat generation (due to the Joule effect) across the domain of the system.

Equations 10.16 and 10.17 are not trivial to be solved either; however, if the velocity profile, V_x^+ , and the temperature profile, θ , could be expressed as functions of two independent variables, the mathematical system can be solved. An interesting approximation, initially proposed by Squire (1938), was used by Turnbull (1969) to represent the velocity field, V_x^+ , and temperature profile, θ , in the analysis of a vertical plate. Adapting this approximation to cylindrical coordinates and axis placement, the following dimensionless terms are given

$$V_x^+ = U^+ \cdot \frac{\eta - b}{\delta^+} \cdot \left(1 - \frac{\eta - b}{\delta^+}\right)^2 \quad (10.18)$$

where U^+ is the dimensionless velocity amplitude in the ξ -direction (x-direction) and δ^+ the dimensionless boundary layer thickness.

$$\theta = \left(1 - \frac{\eta - b}{\delta^+}\right)^2 \quad (10.19)$$

Continuing with Turnbull's approach, after a proper substitution of the proposed velocity and temperature profiles, equations 10.18 and 10.19 respectively, in equations 10.16 and 10.17 followed by integration, the methodology yields the following two first-order differential equations:

$$\frac{\partial}{\partial \xi} \left(\frac{1}{30} \cdot U^+ \cdot \delta^+ \right) = G(U^+, \delta^+, b) + \phi^2 \cdot \delta^+ \quad (10.20)$$

$$\frac{\partial}{\partial \xi} \left(\frac{1}{105} \cdot U^{+2} \cdot \delta^+ \right) = F(U^+, \delta^+, b) + \frac{1}{3} \cdot \frac{Gr}{Re^2} \cdot \delta^+ \quad (10.21)$$

where the following expressions are identified for the auxiliary functions $G(U^+, \delta^+, b)$ and $F(U^+, \delta^+, b)$.

$$G(U^+, \delta^+, b) = \frac{4}{\delta^+} + \left(\frac{2}{\delta^+} + \frac{2 \cdot b}{\delta^{+2}} \right) \cdot \ln \left| \frac{b}{(b + \delta^+)} \right| \quad (10.22a)$$

$$F(U^+, \delta^+, b) = \frac{U^+ \cdot \left[-6b \cdot \delta^+ - 7 \cdot \delta^{+2} - (6b^2 + 8b \cdot \delta^+ + 2 \cdot \delta^{+2}) \ln \left| \frac{b}{(b + \delta^+)} \right| \right]}{2 \cdot \text{Re} \cdot \delta^{+3}} \quad (10.22b)$$

Although a similarity approach has been attempted to obtain an analytical solution for equations 10.20 and 10.21, the effort has been unsuccessful. Therefore, this thesis focuses on the numerical solution. In consequence, if further algebraic development is performed on the previous equations, the following differential system and boundary conditions are obtained.

$$\frac{\partial U^+}{\partial \xi} = -\frac{30}{\delta^+} \cdot (G(U^+, \delta^+, b) + \delta^+ \cdot \phi^2) + \frac{105}{U^+ \cdot \delta^+} \cdot F(U^+, \delta^+, b) + \frac{35}{U^+} \cdot \frac{\text{Gr}}{\text{Re}^2} \quad (10.23a)$$

$$\frac{\partial \delta^+}{\partial \xi} = \frac{60}{U^+} \cdot (G(U^+, \delta^+, b) + \delta^+ \cdot \phi^2) - \frac{105}{U^{+2}} \cdot F(U^+, \delta^+, b) - \frac{35}{U^{+2}} \cdot \frac{\text{Gr}}{\text{Re}^2} \cdot \delta^+ \quad (10.23b)$$

$$U^+ = 0 \quad @ \quad \xi = 0 \quad (10.23c)$$

$$\delta^+ = 0 \quad @ \quad \xi = 0 \quad (10.23d)$$

The resulting model system, represented by equations 10.23 a-d, is trivially solved using conventional numerical methods. For simplicity reasons, the results reported in the next section were obtained using Euler's method, sometimes also called Heun's method (Kreyszing, 1999). The step size of iteration, required by the method, was kept small in order to avoid inaccuracy and imprecision problems.

10.6 Illustrative Results and Discussion

In this sub-section meaningful portrayals are presented for the solution of the model equation describing the cylindrical electrode system. The hydrodynamics taking place in the region near the electrode, the role of Joule heating effect and electrode ratio aspect are studied and analyzed. In particular, plots for boundary layer thickness, temperature profiles, and for the axial component of the velocity field are performed for comparison and discussion. A hypothetical system of fluid with physical properties similar to water has been chosen as a reference. This is necessary to compute reasonable values of dimensionless numbers, Reynolds and Grashof, required by the modeling equations. In addition, valid ranges of physical values have been defined for the source generation term, ϕ^2 and for the electrode ratio aspect, b , as these parameters are important part of the analysis. In consequence, the following ranges have been defined for the parameters of interest.

$$0 \leq \phi^2 \leq 5 \quad (10.24)$$

$$0.1 \leq b \leq 0.5 \quad (10.25)$$

From the range for ϕ^2 and for analysis purposes, four values have been selected as $\phi^2=0$, $\phi^2 = 1.5$, $\phi^2 = 3.0$, and $\phi^2 = 5.0$. The $\phi^2 = 0$ has been included as a reference value for the case of no Joule heating effect. On the other hand, the $\phi^2 = 5.0$ has been selected as a maximum in reference to a similar value considered in the analysis of a rectangular electrode (see previous chapter). The same criteria have been used to select the other two values. For the electrode ratio aspect, b , three values have been selected from the valid domain; these are $b = 0.1$, $b = 0.25$, and $b=0.5$. The criterion in this selection is the use of radius of 20%, 50% and 100%, respectively, of the total electrode length. With the chosen values for ϕ^2 and b , illustration of temperature profiles, boundary layer thickness, and velocity profiles are presented next.

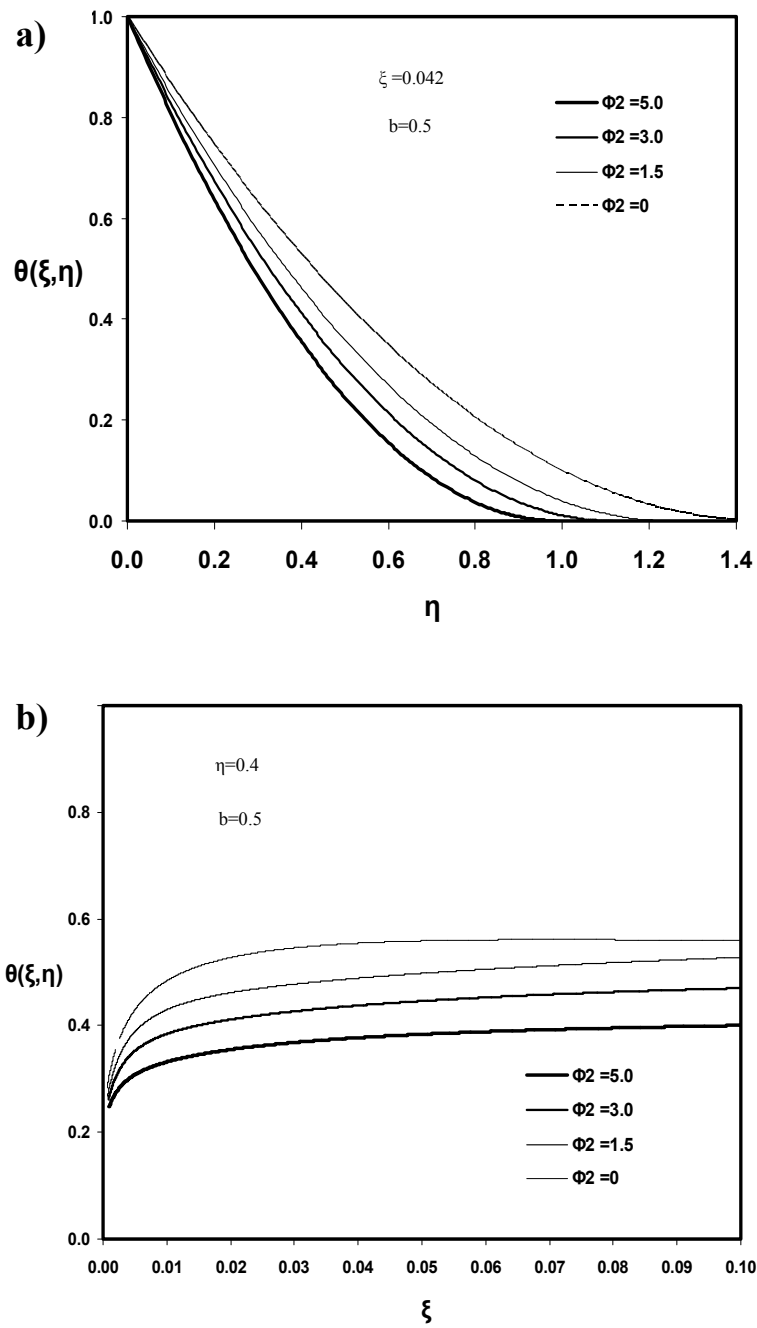


Figure 10.2 Dimensionless temperature profiles (inside the boundary layer) for various values of the heat generation source term. Case of $\xi=0.042$ for the η -direction (a) and case of $\eta=0.4$ for the ξ -direction (b)

Figure 10.2a illustrates a parametric representation of the influence of Joule heating generation on temperature profiles within the domain of the boundary layer. In particular, this figure shows that the range of acceptable ϕ^2 values produces a family of decay type curves, for temperature variation, which are function of the transversal direction of the boundary layer (η) for a given value of axial direction ($\xi=0.042$) and electrode ratio aspects ($b=0.25$). For all given values of ϕ^2 , the temperature at the surface of the electrode ($\eta=0$) remains at the value of $\theta = 1$ and decreases along the radial coordinate to the fluid temperature ($\theta = 0$). A decrease in ϕ^2 values from 5.0 to 3.0 yields an increase on the η value, for $\theta = 0$, from 1.05 to 1.20. From a cross sectional analysis on $\eta=0.6$, the figure predicts that this 40% reduction in ϕ^2 value will cause an increase of approximately 25% in temperature values. Further reduction in ϕ^2 values 70% produces an increase in temperature of 50% approximately. Consequently, the system temperature shows an inverse response and high sensitivity to the Joule heating effect.

Figure 10.2b shows temperature variation along the axial coordinate ξ for a given position of η ($\eta=0.4$) and electrode ratio aspects ($b=0.25$). A general tendency, along the axial coordinate ξ , to describe an inverse exponential function of different amplitudes, for each of the chosen ϕ^2 value, is observed. The higher the value of ϕ^2 the flatter is the amplitude of the curve. In particular, for the electrode region of approximately $\xi > 0.02$, variations in temperature values present a steady increasing slope for all cases of ϕ^2 . This behavior has been also identified on rectangular electrodes.

Figure 10.3 demonstrates the effect of Joule heating on the dimensionless boundary layer thickness along the axial coordinate, ξ , for different values of the source generation term, ϕ^2 and a given electrode ratio aspects ($b=0.25$). Although representing different parameters, the trend observed in this figure is similar to that of figure 10.2b; this is an inverse exponential function. In other words, two main regions are identified. The first is for low ξ values where the exponential function develops. The second region is for ξ values greater than 0.02 where the general variation in the boundary layer thickness, δ^+ , is a straight line with

small slope value. On the other hand, in general an increment in ϕ^2 values from 0 to 5.0 yields a reduction on δ^+ values of 90%. This δ^+ values' behavior is almost linearly proportional for any ϕ^2 value. In other words, the higher the values of the source term ϕ^2 the thinner the boundary layer thickness δ^+ .

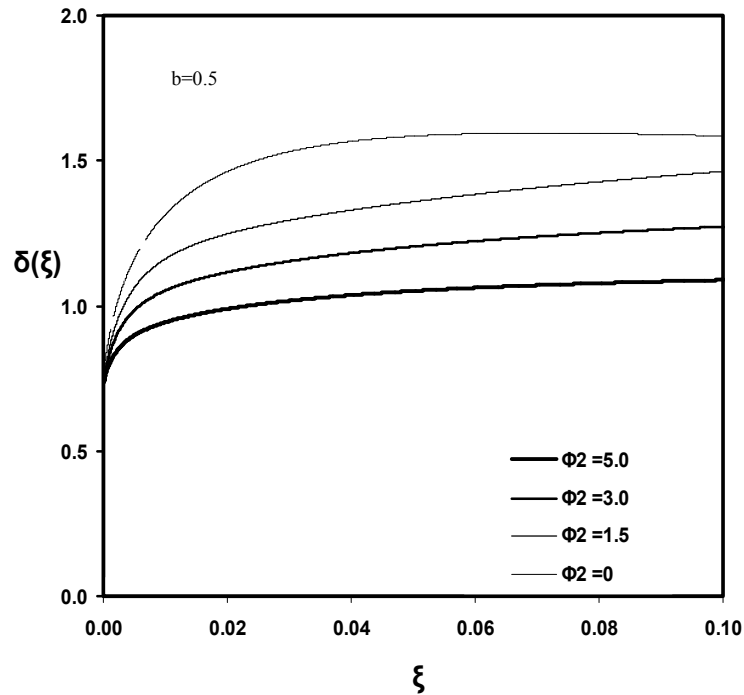


Figure 10.3 Dimensionless boundary layer thickness for different values of the heat generation source term and ratio aspect $b=0.25$.

Figure 10.4a pictures the development of different dimensionless axial velocity profiles induced by Joule heating generation, along the transversal axes, η , inside the boundary layer domain, for a given position in the axial direction ($\xi=0.02$) and electrode ratio aspects ($b=0.25$). The velocity profiles in all the selected ϕ^2 values present a family of curves that mimic a parabolic type shape (as proposed by the Von Karman model) with a slowly decaying end at the region far away from the electrode. Furthermore, for all selected ϕ^2 values the dimensionless axial velocities at the surface of the electrode ($\eta=0$) stay at the value

of $V_x^+ = 0$ in agreement with the imposed non-slip boundary condition. In particular, for a value of ϕ^2 equal to 5.0 the dimensionless axial velocity has a maximum of $V_x^+ = 0.85$ at approximately $\eta=0.3$; this is 1.5 times the value of maximum velocity for the no Joule heating effect ($\eta=0.4$ approximately) and it represents a 50% increase in velocity from the no heating effect case. The same analysis with ϕ^2 value of 3.0 generates a maximum velocity of $V_x^+ = 0.68$ at $\eta=0.35$; this is a 25% increase in the velocity from the maximum velocity for the no Joule heating effect case. Although more examples can be illustrated, it is clear that the system is affected by the Joule heating. In addition, the observed indicates that Joule heating generation will significantly increase axial velocity. Also, the heating effect will reduce the thickness of the corresponding flow stream by as much as 25% ($\phi^2=5.0$) in comparison with the no Joule heating case.

Figure 10.4b presents dimensionless axial velocity profiles variation along the axial coordinate ξ for a given position of η ($\eta=0.4$) and electrode ratio aspects ($b=0.25$). The general trend in velocity profiles, for the different chosen ϕ^2 values, is to develop a straight line type of curve. In other words, higher velocities are expected as the fluid ascends along the axial direction. This behavior is more and proportionally aggravated by higher values of ϕ^2 . Only the no heat generation case describes a small inverse exponential type curve near the cylindrical wall surface that becomes a steady straight line also.

Figure 10.5a demonstrates the influence of the electrode ratio aspect on temperature profiles within the domain of the boundary layer for a given value of Joule heating generation ($\phi^2=3.0$). Particularly, this figure shows identical features to figure 10.2a concentrating in the study of the ratio aspect. In general, higher ratio aspect values produce an almost straight decay line type of curve with temperature development reaching farther from the cylindrical wall position. On the contrary, lower ratio aspect values induce variations that retract the temperature development bending the straight decay line type of curve behavior.

Figure 10.5b shows temperature variation along the axial coordinate ξ for a given position of η ($\eta=0.4$ and Joule heating generation ($\phi^2=3.0$)). In particular, this figure is similar to figure 10.2b in which different cases of electrode ratio aspects have been plotted for

analysis. The general tendency is that higher ratio aspect values promote higher temperature development. These developments are observed to be proportional to electrode ratio aspect values.

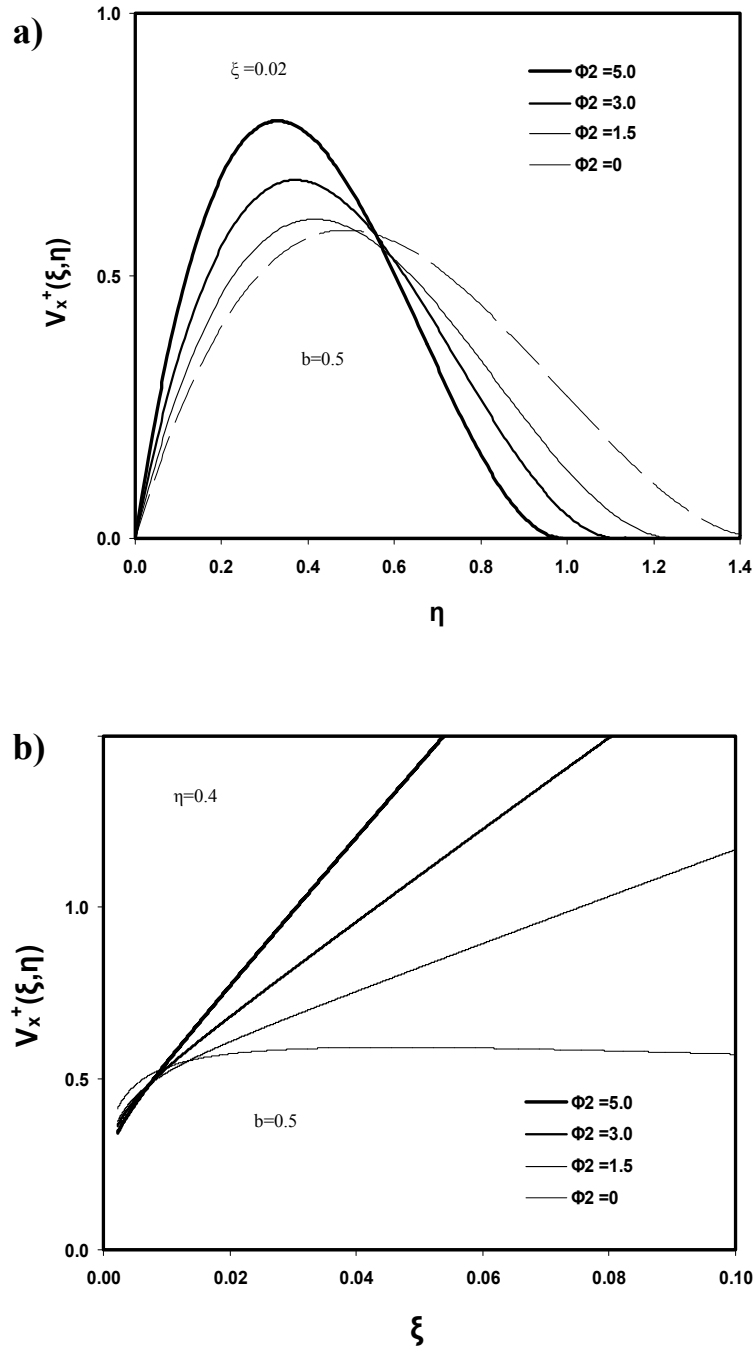


Figure 10.4 Dimensionless total velocity profiles showing the effect of the heat generation inside the boundary layer. Case of $\xi=0.042$ for the η -direction (a) and case of $\eta=0.4$ for the ξ -direction (b)

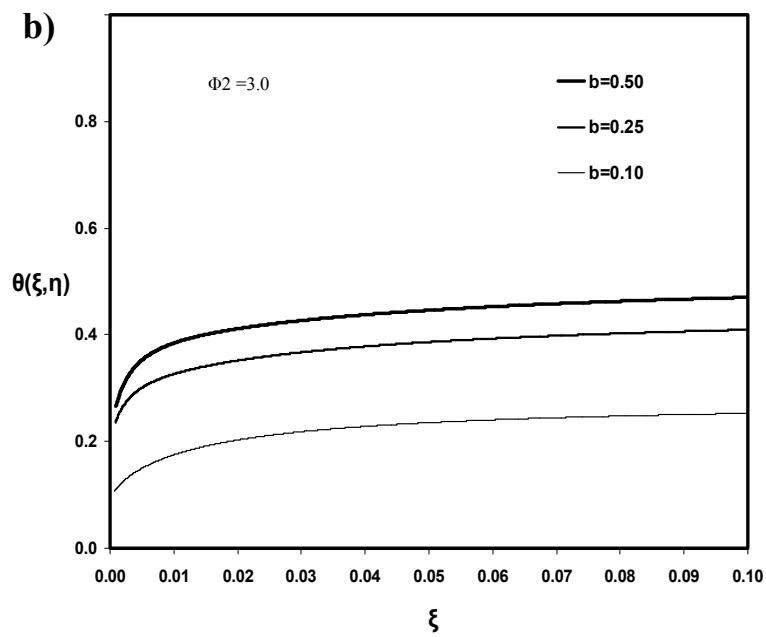
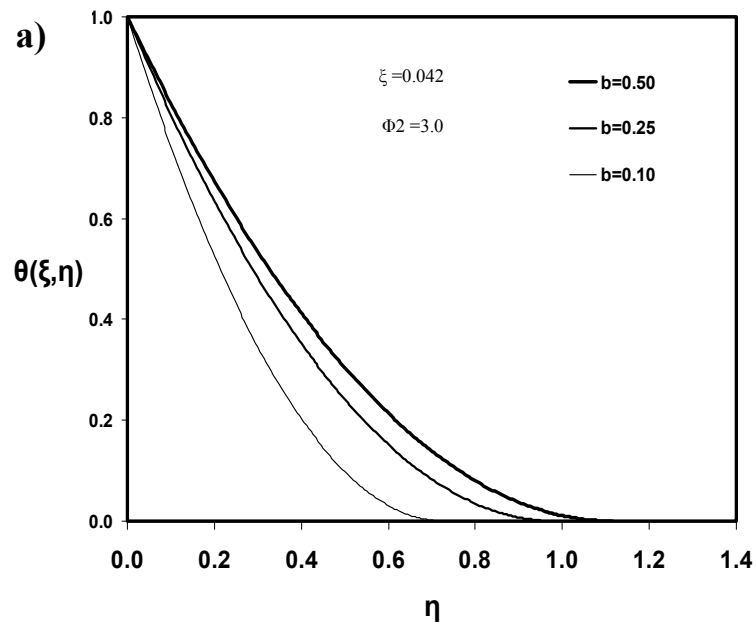


Figure 10.5 Dimensionless temperature profiles (inside the boundary layer) for various values of the electrode ratio aspect. Case of $\xi=0.042$ for the η -direction (a) and case of $\eta=0.4$ for the ξ -direction (b)

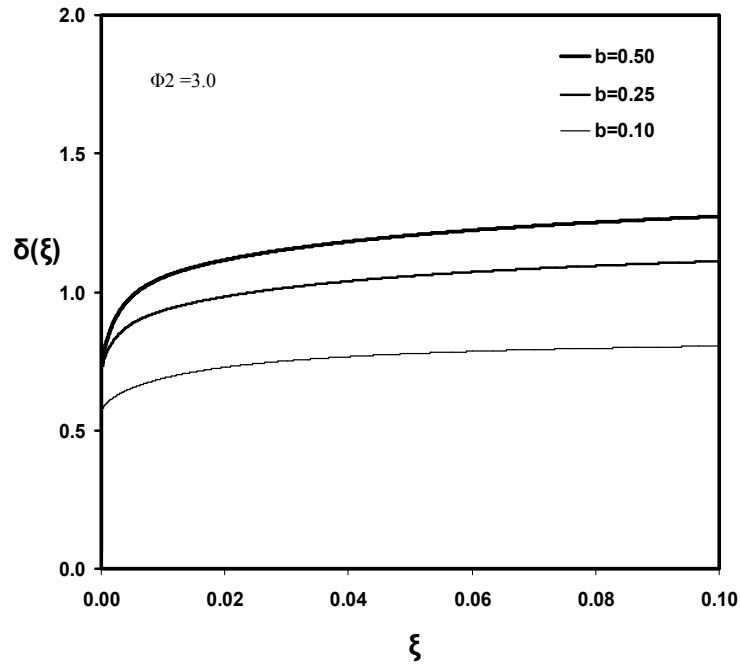


Figure 10.6 Dimensionless boundary layer thickness for different values of the heat generation source term and ratio aspect $b=0.25$.

Figure 10.6 shows the influence of the electrode ratio aspect on the dimensionless boundary layer thickness along the axial coordinate, ξ , for a given value of the source generation term, $\phi^2=3.0$. This figure pictures similar information to figure 10.3 with the additional ratio aspect analysis. The main trend observed in this figure is that increments in “b” values proportionally increase the boundary layer thickness, δ^+ . This enlargement of the boundary layer can be as high as 50% in increment. In other words, the larger the electrode the thinner the boundary layer thickness, δ^+ .

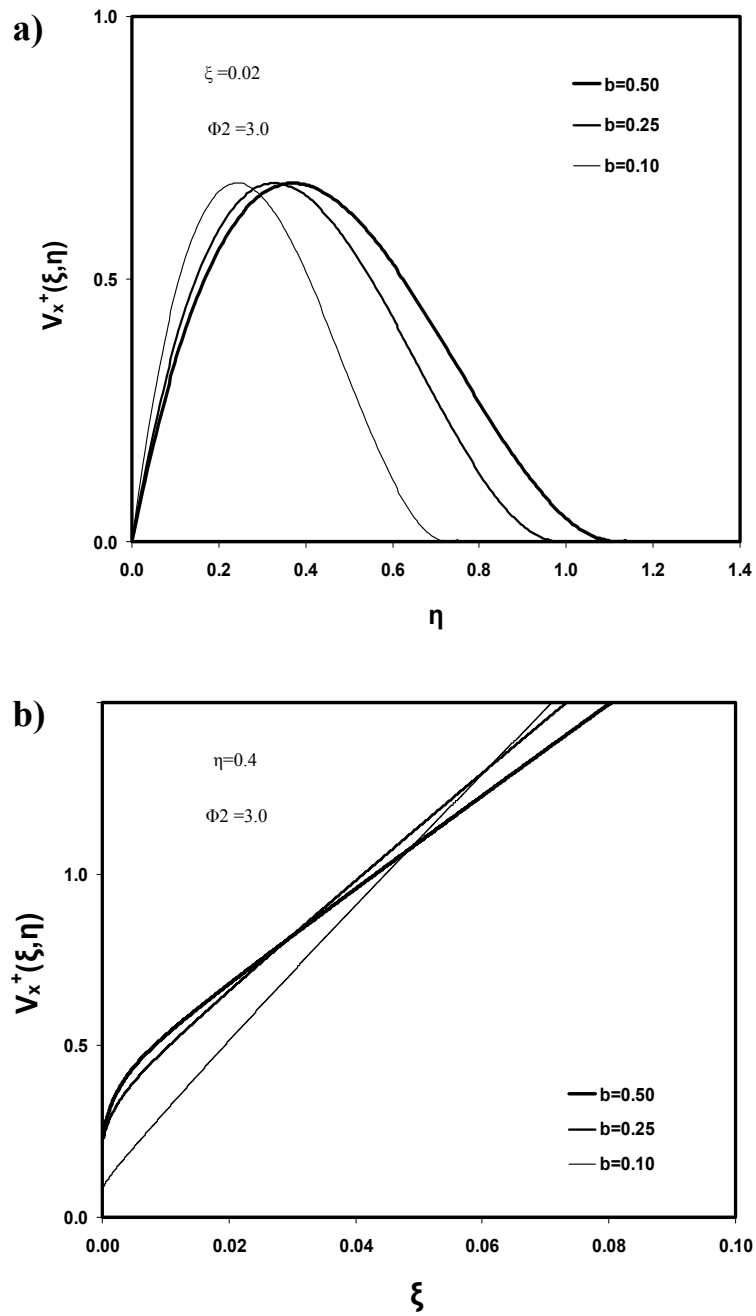


Figure 10.7 Dimensionless total velocity profiles showing the effect of the heat generation inside the boundary layer. Case of $\xi=0.042$ for the η -direction (a) and case of $\eta=0.4$ for the ξ -direction (b)

Figure 10.7a shows the influence of the electrode ratio aspect on dimensionless axial velocity profiles along the radial axes, η , inside the boundary layer domain, for a given position in the axial direction ($\xi=0.02$) and the source generation term, $\phi^2=3.0$. Figure 10.7a is an extension of figure 10.4a for different ratio aspect values. It is interesting to observe that the ratio aspect does not influence the maximum axial velocity values but the thickness of the induced flow stream. In this case, the higher the electrode ratio the thicker the axial flow stream. In other words, ascending to the cylindrical electrode flow regimes should be expected to propagate in the radial direction with shorter electrodes.

Figure 10.7b illustrates the influence of the electrode ratio aspect on dimensionless axial velocity profiles variation along the axial coordinate ξ for a given position of η ($\eta=0.4$) and source generation term, $\phi^2=3.0$. This figure illustrates the same information as in figure 10.4b with the additional portrait of ratio aspect. In this case, the trend is not as clear as in the previous example of velocity profile. In fact, two different trends can be identified. The first trend indicates that near the electrode end ($\xi<0.02$) velocity profiles increase in values as electrode ratio aspect values increase. However, this development is at expenses of lower velocity profiles values beyond the axial point of $\xi=0.02$. In other words, the initial increasing acceleration reaches a steady state; however, the higher the initial acceleration value the lower the steady state acceleration value. Furthermore, longer electrodes should be expected to present steady values of axial acceleration.

10.7 Summary of the Chapter

The present chapter analyzed the hydrodynamics taking place near an electrode of cylindrical geometrical aspect in electrokinetic applications. Furthermore, the analysis is conducted under temperature development conditions where Joule heating effect may be of importance. The applied electrical field around the electrodes during cleaning operations is believed responsible of the heating phenomenon. The subject has been developed as described below.

A boundary layer approach has been used to model the hydrodynamic in the system. Three fundamental equations have been invoked to mathematically describe the system under study. This is the heat transfer model, the continuity equation and the Navier-Stoke equation. The result of this approach is a set of two partial differential equations mutually coupled.

Next, the Von Karman integral approximation is applied to the partial differential equations to simplify the resulting differential system. In addition, simplified velocity and temperature profiles are introduced to facilitate the solution of the integro-differential model. A numerical solution of the differential model equations yields the temperature profile, the boundary layer thickness, and the component of the velocity field along the axial and transversal directions of the vertical electrode.

Finally, the influence of the electrode ratio aspect and heat generation on temperature, velocity profiles and the boundary layer thickness are illustrated for different case scenarios. The effects of electrode length on different parameter space are emphasized.